A two-layer model for landslide generated impulse wave: Simulation of the 1958 Lituya bay landslide impact wave from generation to long–duration transport

Qingquan Liu [a], Menghan Pan [a], Xiaoliang Wang [a,*], Yi An [b]

[a] *Department of Mechanics, School of Aerospace Engineering, Beijing Institute of Technology, Beijing, 100081, China*
[b] *Key Laboratory for Mechanics in Fluid Solid Coupling Systems, Institute of Mechanics, Chinese Academy of Sciences, Beijing, 100190, China*

ARTICLE INFO

ABSTRACT

An updated one-dimensional two-layer coupled mathematical model is developed for landslide generated impulse wave (LGIW) from wave formation to long-duration travel. The coupled model is composed of a landslide model in a bed-fitted coordinate system and a shallow-water wave model in a global coordinate system. The coupling is realized through a reconstruction and interpolation algorithm. We successfully reproduced the experimental reproduction of 1958 Lituya LGIW for a total duration of 250 s at prototype scale, and well captured the three runups on the right bank and three runups on the left bank, together with the six wave crests and troughs in the channel. This seems to be the first reproduction of the Lituya LGIW for such a long duration. The predicted free surface elevation and runups are comparable with experimental results though with some deviations. However, the level of reproduction of the Lituya LGIW from wave formation to long-duration traveling achieved by numerical simulation is greatly enhanced as compared with the existing interface-capture models and mesh-free/particle-based models. This proposed one-dimensional two-layer coupled model could provide a unified framework for LGIWs from generation to long-duration propagation.

1. Introduction

A landslide-generated impulse wave (LGIW) is a major secondary hazard that threatens the safety of a reservoir or coastal infrastructure. The Vajont LGIW that happened in 1963 is a typical hazard (Bosa and Petti, 2011), and the Lituya LGIW in 1958 is an example that took place in a coastal fjord (Fritz et al., 2001). An LGIW involves a cascade of physical processes including wave generation due to landslide–water interaction, and water wave transport for a long distance/duration after. Therefore, models that can simulate an LGIW from generation to long-distance or long-duration transport are valuable for predicting and assessing LGIW hazards in coastal/hydraulic engineering. Recently, experiments (Mohammed and Fritz, 2012; McFall and Fritz, 2016) indicate that two dimensional effects influence the near-field wave characteristics in LGIW. Experimental achievements are not the theme here, which can be found in Heller (2007) and Fritz (2002).

An LGIW is a complex solid–liquid coupling process. The landslide–water interaction introduces a complex and irregular wave, which then travels for a long distance. There are three kinds of numerical models of landslide–fluid coupling in an LGIW. They are interface-capture models where the interface is captured in a mesh-based framework,

mesh-free/particle models for simulating the motions of the landslide and water wave, and two-layer models where both the fluid and landslide motions are integrated over layers. The 1958 Lituya LGIW has become a benchmark for discussing and comparing the performances of these three model types since of the systematic experimental work by Fritz et al. (2001).

In the interface-capture method, the landslide is usually modeled as a non-Newtonian fluid or multiphase flow. Quecedo et al. (2004) pioneered an LGIW model where the landslide is simulated with a Bingham frictional model and the water flow with a Navier–Stokes model, which is later computed with a level set (LS) method. Zhao et al. (2016) contributed to this method using a three-phase model and conservative level set method. In the multi-material model iSALE (Weiss et al., 2009), the landslide is modeled as a plastic material. Basu et al. (2009) used the commercial software Flow3D to simulate the 1958 Lituya LGIW by modeling the landslide as a multiphase flow and capturing the interface with a volume-of-fluid (VOF) method. Mao et al. (2020) developed a discrete element method (DEM) for the landside and coupled it with the water flow via computational fluid dynamics (CFD) using the immersed boundary method. The LS method in Quecedo et al. (2004) obtained a first wave crest of 235 m. Zhao et al. (2016) predicted a first wave crest of 232 m with the LS method. Although they provided a process

---

* Corresponding author.
  E-mail address: wangxiaoliang36@bit.edu.cn (X. Wang).

of wave formation, runup, and back flow, their snapshots (Zhao et al., 2016; Quecedo et al., 2004) showed a landslide flow much like fluid and lost most of the soil structures. This was quite different from the large deformation with soil structures in experiment (Fritz et al., 2001), and they did not fully predict the six wave crests/troughs.

Recently, mesh-free/particle methods have been used to model LGIWs. Salazar et al. (2016) established a particle finite element method (PFEM) with a landslide modeled as a non-Newtonian flow. Shi et al. (2016) developed a coupled soil–water model in a smoothed particle hydrodynamics (SPH) framework to simulate the generation of water waves for both fast and slow landslides, and modeled a landslide as an elastic–plastic material, which is later used to study the near-field characteristics of LGIW in channel-like reservoirs (Wang et al., 2021). They also used the PFEM for a non-Newtonian model of a landslide, which yielded predictions similar to those of the LS method used by Zhao et al. (2016) and Quecedo et al. (2004). The SPH method of Shi et al. (2016) predicts two wave crests and one wave trough using an elastic–plastic model for landsides, which is a bit better than non-Newtonian models. An iSALE model using a plastic material for a landslide predicts two wave crests and one wave trough, comparable with experiment (Weiss et al., 2009) and similar to the prediction of Shi et al. (2016). The only model that has been used to simulate the full 250 s is the VOF model in Flow3D, which treats a landslide as a multiphase flow (Basu et al., 2009); however, the deviation from experiment was quite large because the interaction physics was very different from real physics.

In the two-layer model, both the water wave motion and landslide motion are modeled through depth averaging, where the interaction between the landslide and water is realized through an interface elevation change. Kurganov and Miller (2014) formulated a two-layer model by coupling the Savage–Hutter model (Savage and Hutter, 1989; Yang et al., 2020) and shallow-water model to model a submarine landslide-generated tsunami wave. Pudasaini (2012) formulated a two-phase debris flow model that was later used to simulate a tsunami induced by a submarine debris flow (Pudasaini, 2014; Li et al., 2019) extended the two-layer model to coupling with bed sediment erosion and simulated several small-scale LGIW cases.Ma et al. (Ma et al., 2015) added a dispersion effect to the water flow layer to simulate tsunami wave generation. (González-Vida et al., 2019) used a two-layer model to simulate the whole 1958 Lituya LGIW; however, the treatment of the landslide was approximate and did not predict all crests and troughs. To the authors' knowledge, no two-layer model has ever reproduced the six wave crests/troughs in 250 s for the 1958 Lituya LGIW.

The above survey finds that the VOF/LS model, which treats a landslide as a non-Newtonian material, cannot describe the landslide behavior or interaction physics between the landslide and water. The SPH and iSALE models, which consider the plastic behavior of a landslide, describe a lot of the physics of the landslide and its interaction with water, but can only produce a very short distance for wave transport. Furthermore, the VOF/LS and SPH/PFEM models require very high computation cost, which makes them difficult for making geological LGIW predictions. The VOF/LS and SPH/PFEM models show some ability to simulate wave travel, but the durations in their cases are short because it is more difficult to numerically control dissipation and dispersion for a long time and over a long distance in a Navier–Stokes model than in a wave model. Although DEM-CFD coupling has additional ability to model landslide–water interaction and wave formation, it still has a problem with computing a wave traveling a long distance, making it inapplicable to a geological-scale LGIW.

From the viewpoint of applications, engineers hope to simulate the whole LGIW process in a unified framework and extract free surface elevation at typical positions such as dam site for design. However, this task is not fulfilled. Although the recent experiments (Mohammed and Fritz, 2012; McFall and Fritz, 2016) and numerical simulation (Wang et al., 2021) indicate two dimensional effects influence the near-field characteristics of LGIW, as a first step, this study

aims to develop a one-dimensional two-layer LGIW model from wave formation to travel for a long duration/distance in a unified framework, in the hope that it can be extended to a geological-scale LGIW.

2. Coupled model for an LGIW and numerical algorithm

In this section, we construct the coupled LGIW model and present the key reconstruction and interpolation algorithm.

2.1. Model development and components

An LGIW is a coupled dynamical process composed of a landslide on a steep slope and a traveling water wave (Shi et al., 2016). Generally, the coupling starts between the landslide and water wave generation phase and stops after the landslide ceases. From an engineering standpoint, a coupled model should also be computationally effective and extendable to the engineering scale. Satisfactory progress has been achieved in modeling water waves, such as the shallow-water model for long waves and Boussinesq model for dispersive waves (Lanne, 2013), and modeling of landslide dynamics is not far behind (Pudasaini and Hutter, 2007). From point of application, engineers wish to simulate this coupled process in a unified framework and extract key information such as free surface elevation in front of a dam. However, there is still no such coupled models. Therefore, in this study, we attempted to develop such a model in one-dimension which couples landslide dynamics and wave propagation in long duration.

As shown in Fig. 1, we use a shallow-water model for water wave transport in a global coordinate system. Landslide dynamics strongly depends on topographic constraints. We formulate landslide dynamics in a local bed-fitted coordinate system because this better accounts for topographic effects (Pudasaini and Hutter, 2007), which is easy to solve. For simplicity, the landslide here is assumed to be a rigid body, which could be extended to a deformable model (Pudasaini and Hutter, 2007; Yang et al., 2020; Wang and Liu, 2021). To make the formulation of the coupled system clear, we split the shallow water model in a global coordinate system and landslide dynamics in a bed-fitted system as shown in Fig. 2(a) and (b). The coupling between the water wave and landslide is realized through updating bed topography.

As shown in Fig. 1, and Fig. 2(a), the one-dimensional dynamics of shallow water is formulated in a global coordinate system (*xoz*) as in Eqs. (1-2).

$$\frac{\partial h}{\partial t} + \frac{\partial hu}{\partial x} = 0, \tag{1}$$

$$\frac{\partial hu}{\partial t} + \frac{\partial (hu^2 + 0.5gh^2)}{\partial x} = -gh\frac{\partial (z_b + z_s)}{\partial x}, \tag{2}$$

where h and u are the water depth and velocity respectively, g is the acceleration due to gravity, and z_b and z_s are the bed elevation and slide depth respectively. It is remarked that here all the physical variables are the functions of (*x,t*).

We then formulate the landslide dynamics in unit mass in a bed-fitted system (ξ,t) using Newton's second law as shown in Eq. (3), where the landslide is assumed as a rigid body in the bed-fitted system. After transformation its local height into the global depth, the landslide model could exhibit deformation due to the bed curvature, however it will still preserve rigidity if the landslide scale is much smaller than the bed curvature scale.

$$\begin{cases} \frac{dV_s}{dt} = f_{grav} + f_{fric} + f_{drag}, \\ \frac{d\xi_c}{dt} = V_s \end{cases} \tag{3}$$

where ξ_c and V_s represent the center and velocity of the rigid landslide. The forces for unit mass acting on the landslide are gravity f_{grav}, friction f_{fric}, and drag f_{drag}, as seen in Fig. 2(b). Since the landslide is assumed rigid, we only needs to account the forces acting on its center. It is remarked all the force variables are the functions of (ξ,t). The
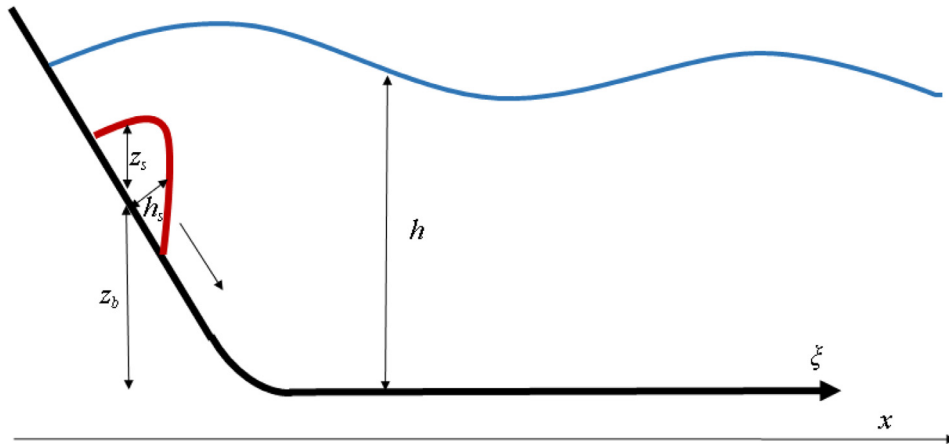
Fig. 1. Illustration of an LGIW. The red line represents a landslide in a bed-fitted system, and the blue curve is a water surface.
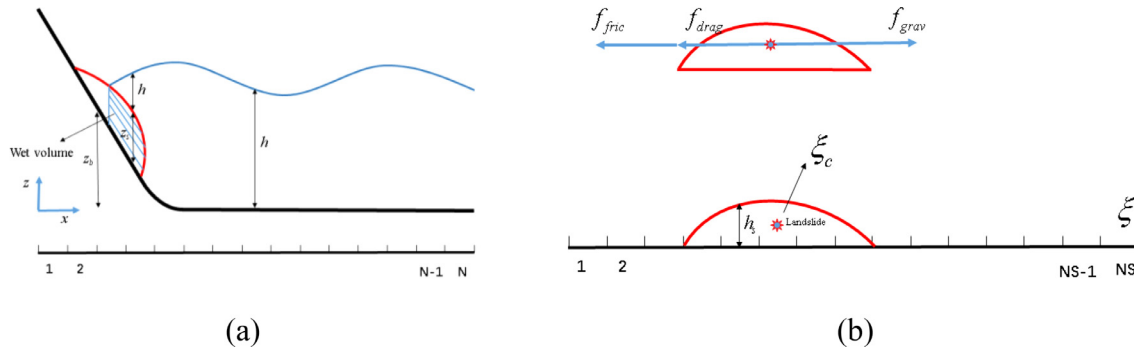

Fig. 2. Details of shallow water wave in global coordinate system (a), and landslide dynamics on a bed-fitted coordinate system (b).

governing equation for the rigid body landslide is an ordinary differential equation as compared with the partial differential formulation for deformable landslides and avalanches (Savage and Hutter, 1989; Yang et al., 2020; Wang and Liu, 2021). Once the center of the landslide is known, one could easily construct the local height distribution h_s as shown in Fig. 2(b). Here h_s is also the function of (ξ,t). The governing equation in Eq. (2) with the initial position and velocity formulates an ordinary differential equation (ODE) model for the landslide dynamics.

The formulae for the gravitational forces in air, f_{grav}^a, and water, f_{grav}^w, are

$$f_{grav}^a = g \sin(\theta), \tag{4}$$

$$f_{grav}^w = \frac{\Delta\rho}{\rho} g \sin(\theta), \tag{5}$$

where $\theta(\xi)$ denotes the bed inclination angle.

We formulate the frictional forces in air, f_{fric}^a, and water, f_{fric}^w, as in landslide dynamics (Pudasaini and Hutter, 2007; Blasio, 2011) to account for bed curvature, buoyancy, and granular liquefaction:

$$f_{fric}^a = -(1 - r_{pa})(g \cos(\theta) + \frac{V_s^2}{r}) \tan(\delta) sign(V_s) \tag{6}$$

$$f_{fric}^w = -\frac{\Delta\rho}{\rho}(1 - r_{pw})(g \cos(\theta) + \frac{V_s^2}{r}) \tan(\delta) sign(V_s), \tag{7}$$

were r_{pa} and r_{pw} represent the liquefaction indexes in air and water for a large-scale landslide, ρ is the density of the landslide, $\Delta\rho$ is the density difference in water for a landslide, V_s is the velocity of the landslide in the local bed-fitted system, δ is the bed friction angle, and the term $\frac{V_s^2}{r}$ represents centrifugal force where r is the bed curvature radius.

In contrast to models using a purely Coulomb friction model (González-Vida et al., 2019; Weiss et al., 2009), introducing a liquefaction index is very important for accounting for fluidization of a giant

landslide involving a mass of more than 10^6 m³ (Blasio, 2011; Iverson et al., 1997). Without that, the friction angle selected should be much smaller than the typical value for granular materials to match the runout of giant landslides (González-Vida et al., 2019; Wang and Li, 2017; Weiss et al., 2009). However, the physical mechanism of long runout behavior of a giant landslide is still an open question (Blasio, 2011; Iverson et al., 1997).

The drag force under water is composed of surface frictional drag and pressure drag (Blasio, 2011) and is expressed as

$$f_{drag}^w = -\frac{1}{2} \frac{\rho_w}{\rho} (\frac{C_d}{L_s} + \frac{C_s}{H_s}) V_s^2 sign(V_s), \tag{8}$$

where ρ_w is the water density, C_s and C_d are the surface friction and pressure drag coefficients, L_s and H_s are length and height of the landslide. Air drag is ignored.

The entry of landslide into water is a very complicated physical process which involves impact, solid-fluid coupling effects, water wave rolling, wave break et al. (Blasio, 2011; Fritz et al., 2001; Heller, 2007) The theory and numerical methods for this process are still not well developed in both 3D models (Zhao et al., 2016; Shi et al., 2016) and the depth-averaged model. In the present study, both water wave and landslide are simplified in a depth-averaged way to simulate the overall behavior of LGIW including the entry process. Therefore, to be as simple as possible, the force of the landslide going into water is calculated via an average of the forces in air and water using the weight of the wet volume fraction as shown inEq. (9). To consider the dynamical effects and make it consistent with force in pure air or water, the dynamical wet volume in Fig. 2(a) is chosen rather than wet volume in mean water stage.

$$f = (1 - \omega) f_j^a + \omega f_j^w, \tag{9}$$

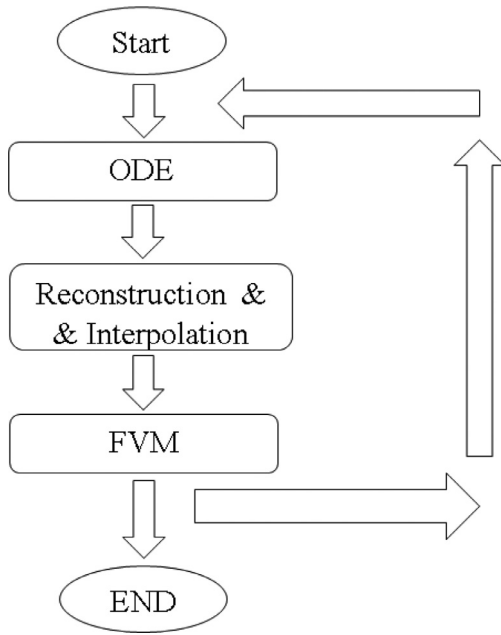where j represents gravity, friction, and drag, and ω is the wet volume fraction.

Fig. 3. Computational procedure for a landslide-generated impulse wave, ODE solver is for landslide in local bed coordinate system, FVM solver is for shallow water model, and Reconstruction && Interpolation solver is for coupling between landslide and shallow water wave.

The interaction between the water wave and landslide motion is included via the landslide depth z_s as could be found in Fig. 2(a).

Remarks: Physics of landslide dynamics is not well understood as that of water waves, which leads to various kinds of formulations for landslide dynamics. We formulate the landslides models in a bed-fitted coordinate system which could reflect the bed curvature effects, steep terrain effects, and nonhystatic effects better than the classical shallow water formulation (Pudasaini and Hutter, 2007; Wang et al., 2021; Yang et al., 2020). To be coincide with the classical shallow water wave models, the landslide models in most of the existing two-layer models (González-Vida et al., 2019; Kurganov and Miller, 2014; Li et al., 2019; Pudasaini, 2012) for LGIW rely on the hydrostatic assumption in a global coordinate system, which may cause severe errors in landslide process and its later effect on LGIW (Castro-Orgaz et al., 2015; Ni et al., 2019; Wang and Liu, 2021).

2.2. Essential numerical ideas

As shown in Section 2.1, the coupled model includes an ordinary differential model for landslides in Eq. (3) and a shallow-water model for the water wave in Eqs. (1-2), which are coupled through the landslide depth z_s. The computational procedure is divided in Fig. 3 into three components including an ODE solver for the landslide, an FVM (finite volume method) solver for the shallow-water flow, and a reconstruction and interpolation solver which transforms the landslide depth $h_s(\xi(t))$ in the local bed-fitted system into the depth in global system $z_s(x,t)$. We choose a second-order Runge–Kutta scheme for the ODE solver. The shallow-water wave model is a nonlinear hyperbolic system that includes shock waves, a wetting/drying front, and a well-balance problem, requiring careful calculation. Constructing the landslide depth from the moving landslide is the key problem in this procedure and is presented in Section 2.3.

We use a recently developed hyperbolic scheme (Kurganov and Petrova, 2007; Huang et al., 2020) to solve the shallow-water problem. The advection term is solved with a Riemann-free solver first proposed by Kurganov and Petrova (2007) by reformulating an early staggered solver into a collocated mesh. The well-balance behavior is realized by

reconstructing the bed and water depth (Audusse et al., 2004; Huang et al., 2020). The wetting–drying front is captured with a wetting–drying technique (Liang and Marche, 2009; Wang and Li, 2017). We use N cells for the shallow water wave model as shown in Fig. 2(a).

2.3. Landslide surface reconstruction scheme

As stated in Section 2.2 and also shown in Fig. 2 (a-b), the coupling between the landslide and water wave is realized by updating the bed depth $z_s(x,t)$ in global coordinate system. After solving the landslide dynamical model for one time-step, we construct the new depth distribution $h_s = h_s(\xi(t))$ by simply moving its center in last time step to its current position in the local bed-fitted system, where the cells for the landslide model is NS as shown in Fig. 2(b). Then we transform the landslide height $h_s(\xi(t))$ in the local coordinate system into the landslide depth $z_s(\xi,t)$ in the global coordinate system to close the computational procedure. We first reconstruct the landslide depth in global coordinates as $\tilde{z}_s = \tilde{z}_s(\tilde{x})$, and $\tilde{x}$ and $\tilde{z}_s + \tilde{z}_b$ are the reconstructed coordinates of the surface points. Here we omit the time variable t. Then we interpolate between $\tilde{x}$ and x to find the landslide depth z_s consistent with the global mesh x for the shallow-water solver as in Eq. (10).

$$\begin{aligned} \tilde{x} &= x + h_s \sin(\theta) \\ \tilde{z}_s + \tilde{z}_b &= z_b + h_s \cos(\theta) \end{aligned} \tag{10}$$

where $\theta(\xi)$ is the bed inclination. The first step of Eq.(10) is termed the reconstruction step, and the second is the interpolation step.

We combine these steps together as reconstruction and interpolation to close the LGIW computational procedure in Fig. 4.

3. Verification examples

Three examples are now presented to verify the coupled model. Section 3.1 presents well-balance behavior, 3.2 is for dam break flows, and 3.3 is for a moving bottom-induced water wave.

3.1. Well-balance behavior

The shallow-water model in Eqs. (1-2) has a hydrostatic solution ($h + z_b = const, u = 0$) that balances the source term and flux term. Such a solution coincides with a hydrostatic distribution without velocity. This structure should be numerically retained and is termed the well-balance problem. The wetting–drying front exists when the bed height is higher than or equal to the water elevation. An example is when water elevation is lower than an island crest, which must be also well captured. Therefore, we simulate two extreme examples of hydrostatic flow over a smooth island and a discontinuous island. In both cases, the hydrostatic water elevation is 3 m, and the computation is 50 m long. The bed functions of the two cases are

$$z_b = \begin{cases} 5.0 \exp(-(x-25)^2) & |x-25| < 5 \\ 0 & |x-25| \geq 5 \end{cases}, \tag{11}$$

$$z_b = \begin{cases} 5.0 & |x-25| < 5 \\ 0 & |x-25| \geq 5 \end{cases}. \tag{12}$$

The computational results for water surface elevation and discharge are shown in Fig. 5(a) and (b) respectively. The well balance is preserved for hydrostatic flow over an island. In addition, the wetting–drying front near the bank is also well captured. The discharge near the wetting–drying front is kept within a very small value.

3.2. Dam break wave front

In an LGIW, the wetting–drying interface and wave front exist frequently. We simulated a dam break flow involving these two features. The initial condition is

$$(h,u) = \begin{cases} (10,0) & x < 0 \\ (0,0) & x > 0 \end{cases}. \tag{13}$$

$$h_s = h_s(\xi)$$

Reconstruction

$$\tilde{z}_s = \tilde{z}_s(\tilde{x})$$

Interpolation

$$z_s = z_s(x)$$

Fig. 4. Reconstruction and interpolation for the coupling between the landslide model and shallow-water model.
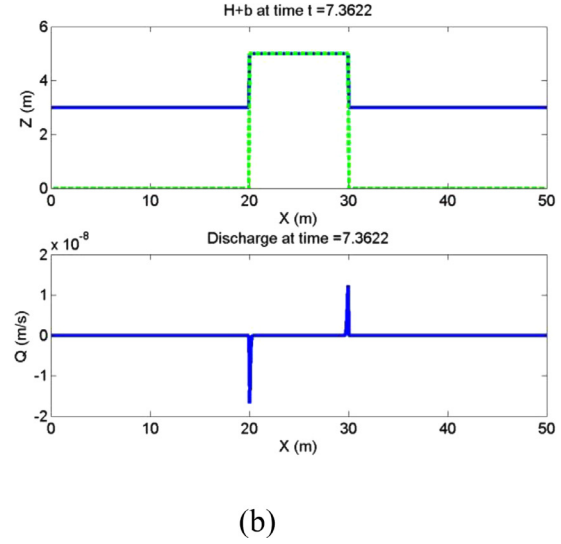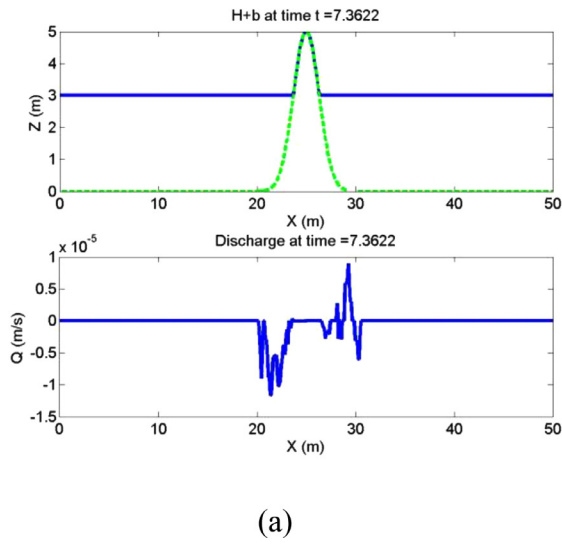

(a)

(b)

Fig. 5. Well-balance behavior of the shallow-water model over (a) a smooth island and (b) a discontinuous island. Z represents the water surface elevation, and Q denotes the flux per unit width.
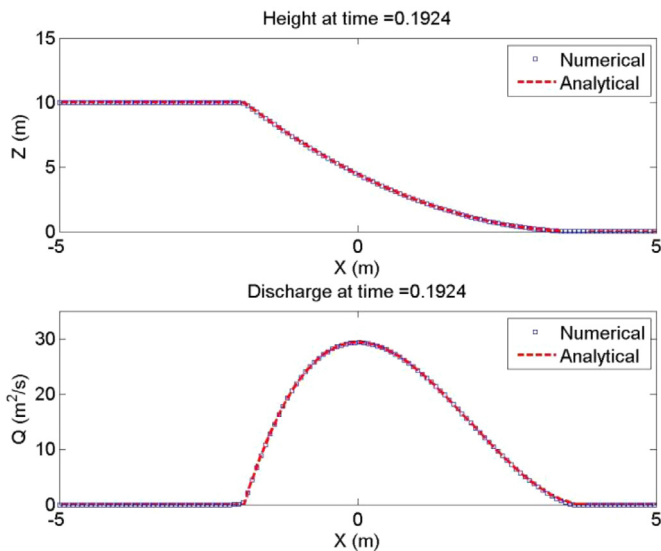

Fig. 6. Comparison between numerical simulation and analytical solution for a dam break flow over a flat bed. Z represents the water surface elevation, and Q denotes the flux per unit width.

This dam break flow has a similar solution that could be easily obtained through Riemann-invariant theory (Billingham and King, 2000) as

$$(h, u) = \begin{cases} (h = \frac{h_0}{9}(2 - \frac{x}{ct})^2, u = \frac{2}{3}(c + \frac{x}{t})) & -ct < x < 2ct \\ (h_0, 0) & x \le -ct \\ (0, 0) & x \ge 2ct \end{cases},$$

(14)

where h_0 is the initial height, and $c = \sqrt{gh_0}$ is the gravitational wave speed. As Fig. 6 shows, our simulation well captures the dam break flow and computes a good front.

3.3. Surface wave caused by a moving bottom bump

A moving bottom induces several beautiful wave patterns because of the interaction between the bottom and water wave. For a very small amplitude, a linear wave approximation is appropriate for a traveling wave and has the analytical solution obtained by Tinti et al. (2001). We simulated one linear case and one nonlinear case. Three dimensionless numbers govern the coupled wave: $Fr = \frac{u_s}{\sqrt{gh_0}}$, $\mu = \frac{h_0}{L_s}$, and $\mu_s = \frac{H_s}{L_s}$, where u_s is the bump moving velocity, h_0 the initial water depth, H_s the landslide height, and L_s the landslide width. The landslide is modeled as a rigid parabolic bump moving right and initially set at $x = 125$ m in Fig. 7.

In the linear case, the physical parameters are $Fr = 0.2$, $\mu = 0.2$, and $\mu_s = 0.05$. The numerical solver successfully captures the three-wave structure (Tini et al., 2001) including a leading wave, a trapped wave, and a tailing wave due to slight bottom bump motion. This agrees well with the analytical solution, as shown in Fig. 7(a).

In the nonlinear case, the physical parameters are $Fr = 0.2$, $\mu = 0.2$, and $\mu_s = 0.5$. In this case, transcritical flow happens on the back of the bump that induces a shock on the back of the bump, as shown in Fig. 7(b). The linear solution fails in this case but still yields an approximation for a tailing wave, as shown in Fig. 7(b).

4. Application to the 1958 Lituya bay lgiw

We simulated the 1958 Lituya bay LGIW. We analyzed in detail the wave generation, runup, and back-flow behavior and compared the results with typical simulation results of the VOF, SPH, and LS methods to show the advantage of the present model.

4.1. Physical setup

The Lituya Bay LGIW happened on July 8, 1958, and was caused by an earthquake that triggered a major subaerial landslide rush into the Gilbert Inlet at the head of Lituya Bay (Fritz et al., 2001). This LGIW had many two-dimensional (2D) features due to the geometry of the landslide and inlet. Fritz et al. (2001) carried out a series of indoor flume
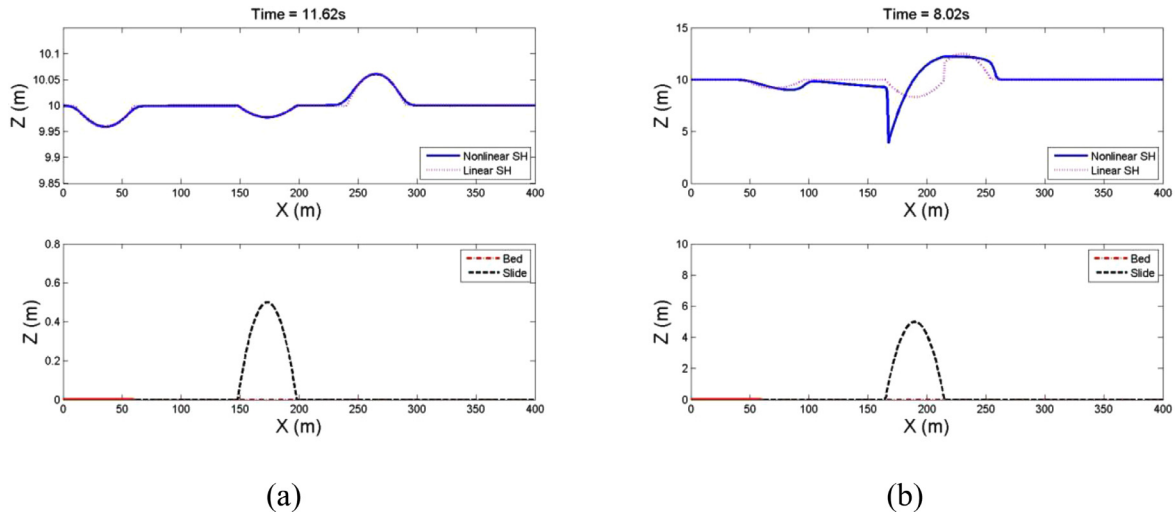
Fig. 7. Moving bottom-induced surface wave: numerical versus analytical solution. (a) Linear nondispersive surface wave for a small disturbance. (b) Shock formation for a nonlinear disturbance.
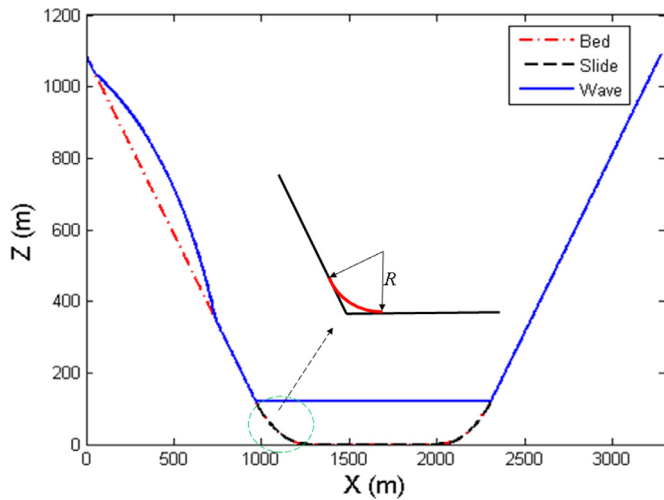

Fig. 8. Setup of the Lituya bay LGIW, the left and right corners are smoothed by an arc of radius R.

experiments to study the wave generation and runup behavior, and provided useful pictures and free surface elevation data. This case has been tested with many algorithms such as the VOF (Basu et al., 2009), SPH (Shi et al., 2016), multi-material finite difference (Weiss et al., 2009), and LS methods (Zhao et al., 2016). We simulated this problem with the present model.

The physical setup is shown in Fig. 8, where the initial water depth is 122 m, and the left and right banks are inclined at 45° to the horizontal. To make the setup consistent with our model, we smoothed the two corners with circular arcs tangent with both banks and the flat bottom. The tangent point with the bank is the crossing node between hydrostatic water level line and the bank line with a radius of 417 m. The landslide was initially set upstream on the left bank. The computational domain for the water wave model in the global coordinate system in x direction is from 0 to 3274.2 m, and the domain for the landslide model in the local bed-fitted system in ξ direction is from 0 to 4133.6 m. We used the physical parameters of Fritz et al. (2001) in our model as much as possible. The initial position of the center for the landslide is 556 m in global coordinate system and 786.3 m in local bed-fitted system correspondingly. The initial velocity is zero. The length and height of the landslide were 970 m and 92 m respectively, which forms a parabola

downward. The density of the landslide was 1.6 kg/m^3 with a void fraction of 39%. We used a friction angle typical of a 40° granular material according to experiment (Fritz, 2002; Shi et al., 2016), which is different from that of a pure Coulomb friction model where only a very low friction could generate a runout matching experiment (González-Vida et al., 2019; Wang and Li, 2017; Weiss et al., 2009). The pressure and friction drag coefficients were set to typical values for a slender body: $C_d = 0.2$ and $C_s = 0.1 C_d$ (Blasio, 2011). We have pointed out that an LGIW is a very complex process involving soil–water interaction, especially for giant landslide-induced waves. Therefore, in-depth uncertainty analysis or quantification of the input physical/geological parameter values should be conducted to diminish the uncertainty (González-Vida et al., 2019). However, we chose typical values for parameters such as the friction angle and drag coefficient that have a solid foundation in both theory and experiment in soil mechanics and fluid mechanics. For the fluidization index, which accounts for the long runout of a giant landslide in our model, we used trial and error to obtain $\lambda_{pa} = 0.5$ and $\lambda_{pw} = 0.1$.

The combined physical model produces a landslide front moving toward the right corner with some material rushing onto the right bank. In the experiment, the landslide finally stopped at the right corner. The deviations between the present model and experiment are due to modeling the landslide as a rigid body without considering the deformation and contraction in front of the landslide, which was estimated to be 748 m before impact (Fritz et al., 2001). The whole process of this LGIW was successfully reproduced thanks to the short duration of the wave generation phase, as we will show in Sections 4.3 and 4.4. The free surface elevation detection point was set at $x = 1850$ m, corresponding to the wave gage at 885 m from the left water surface in the original experiment. In addition, the runups on both the left and right banks were recorded.

4.2. Mesh dependence and smoothing radius effect

We analyzed the mesh dependence for this problem because there are two meshes: one for the landslide in the bed-fitted system, and another for the shallow water in the global coordinate system. The mesh combination (N, NS) shown in Fig. 9 was examined, where N denotes the mesh for the shallow water, and NS represents the mesh for the landslide as also shown in Fig. 2. Eleven cases with different mesh combinations from (100, 100) to (2500, 2500) were simulated for a duration of 250 s.

Fig. 9 shows the free surface elevation at the gage point for four typical cases. There are six crests and six troughs for the whole process. The result converges most of the time except for the second and fourth
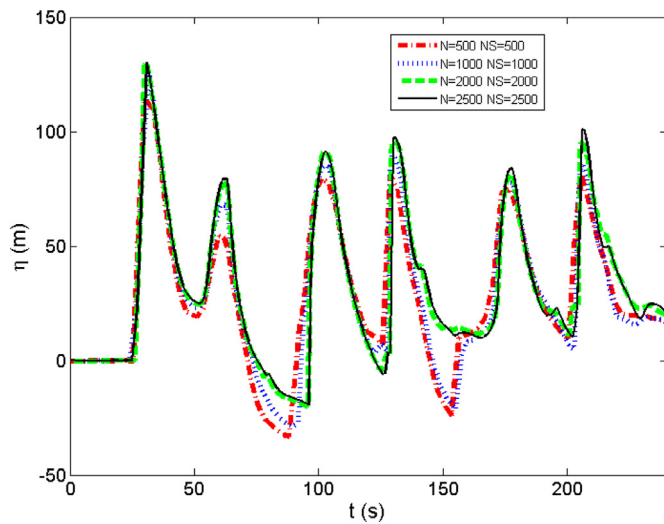
Fig. 9. Mesh dependence for the free surface elevation at the gage point. N and NS are the meshes for the shallow-water and landslide models.
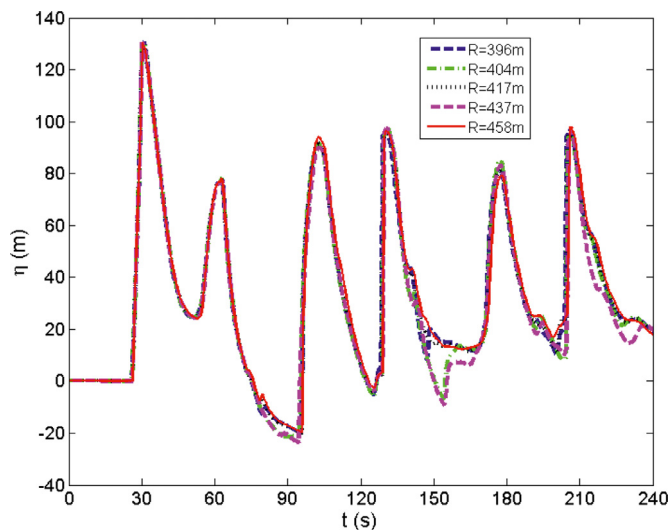

Fig. 10. Influences of the smoothing radius of the two corners on the free surface elevation at the gage points.

Fig. 11. Free surface elevation at the gage point and comparison with the VOF, SPH, and level set methods.

use the standard smoothing radius of 417 m in which the tangent point is on the initial hydrostatic water level.

4.3. Wave height and runup

As shown in Fig. 9 and 10, we captured the six wave crests and troughs in the whole 250 s. We compared the predicted free surface elevation at the gage point with the experimental and simulated results from several methods presented in the literature, such as the VOF method using Flow3D (Basu et al., 2009), SPH method (Shi et al., 2016), and level set method (Zhao et al., 2016), as shown in Fig. 9. We have pointed out that the free surface elevation at the gage point obtained with iSALE (Weiss et al., 2009), where the elastic–plastic behavior of the landslide is considered, agrees well with the SPH result obtained by Shi et al. (2016) for a duration of about 60 s. We only choose the SPH model for comparison. As shown in Fig. 11, only the present model and the VOF method show the full 250 s process. SPH only gives the first two crests and the first trough, while the level set method only yields data for the first wave. The present model captures the six wave crests and six wave troughs with a resulting free surface elevation at the gage point comparable with the experimental result, especially for the first three crests and three troughs. However, the VOF study used a multiphase flow model for the landslide that had very large deviations, especially for the six troughs, which is due to the fake fluidization of the landslide simulation in that model. The impact obtained in the SPH and level set methods seems better than in the present method because the full physical process is accounted for, but the long-time transport and back-flow data are not given, which might be due to the large dissipation in these methods for long-distance transport. Similarly, landslide motion in the level set method (Zhao et al., 2016) deviates a lot from experiment for very high fluidization owing to the use of a non-Newtonian model. However, the SPH model, which accounts for the elastic–plastic behavior of a granular landslide as well as the iSALE model (Weiss et al., 2009), has a much smaller deviation in fluidization for landslide motion than the non-Newtonian and multiphase models. The last three crests and troughs have some deviations from experiment in our model, but are still much better than the only VOF simulation. We believe that considering dispersion and dissipation effects in the present model could reduce these deviations.

Fig. 12 shows the wave runup on the right bank and comparison with the experimental, VOF, and SPH results. SPH only gives the first runup, which seems better than in the other two methods. The present model predicts a lower first runup than experiment, while VOF shows a

trough for meshes up to (1000, 1000). However, only a mesh combination over (2000, 2000) is enough for convergence with all six wave crests and troughs. Therefore, the following simulation results are for the mesh (2000, 2000).

Since the smoothing radius for the two corners also affects the coupled dynamics, we performed several cases with different smoothing radii around the standard smoothing radius within 10% deviation. The free surface elevation time series at the detection points are shown in Fig. 10. It implies that most of the free surface elevation at the six crests coincide with each other, the free surface elevations do not change a lot for the first three troughs. However, it is found that for the 4th to 6th troughs, especially the 4th trough, the computational model exhibits some deviations for the smoothing radii. Since this problem involving severe nonlinear coupling effects among wave propagation, landslide dynamics, and their coupling which add difficulties to the numerical method, we still believe that the proposed model is acceptable, at least for the LGIW engineers since who mainly design dams by evaluating the free surface elevation at crests. In addition, the smoothing radius is much larger the height of the landslide (90 m). In the later cases, we
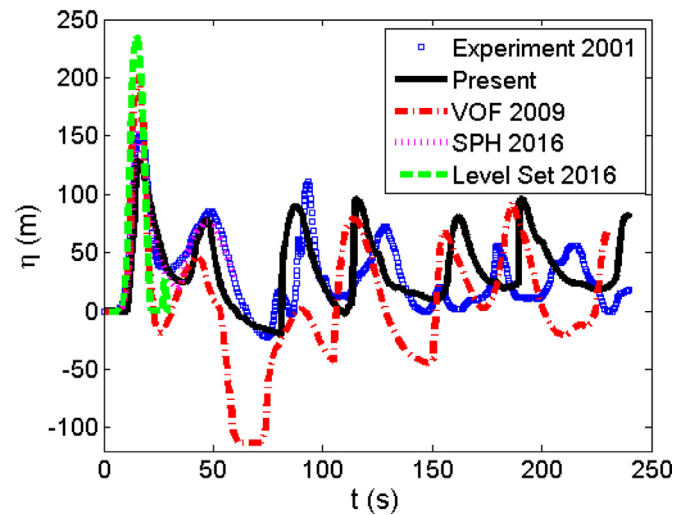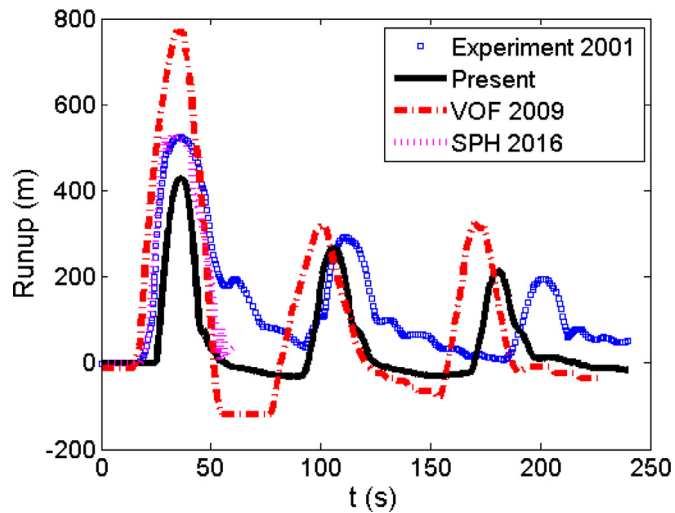
Fig. 12. Runup on the right bank and comparison with VOF, SPH, and level set methods.
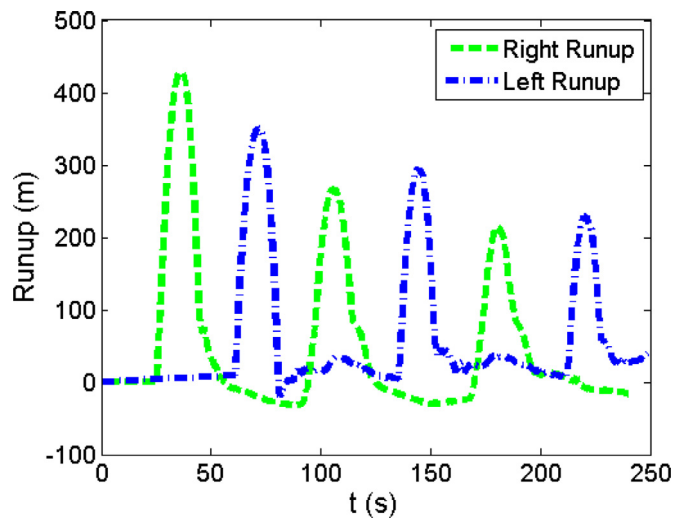

Fig. 13. Comparison between runups on the left and right banks.

greater first runup. As for the second and third runups, the present model predicts with a time delay but is still better than the VOF methods. The SPH method did not provide the later runups.

Fig. 13 also shows the three runups on the right bank and three runups on the left bank. The runups on both banks decrease with time although there is no friction term in the current shallow-water model. The energy dissipates owing to shock formation in the channel, which in the real world might be even caused by wave breaking. Therefore, we believe that considering friction and dispersion effects would enhance the predictive ability of the present model for an even longer time.

4.4. Physical process

Fig. 14 shows six typical snapshots to clarify the complex wave generation, runup, and back flow. Panels (a) and (b) show the impact of the landslide on the quiet water and sudden elevation of the water. The water wave does not have time to transport owing to the short duration, but a surge forms in front of the landslide similar to the leading wave induced by the moving bottom bump in Fig. 7. The effect of elevation or gravity is considered in the interaction without a flow separation appearing, which is a bit different from experiment. As the landslide moves further, the surge persists and moves towards the right bank. In

Fig. 14(d), the landslide almost ceases, and the surge climbs up on the right bank, falls back as shown in Fig. 14(e), and then back-flows and runs up on the left bank in Fig. 14(f). A shock in the channel is found moving back and forth in Fig. 14(e) and (f) to dissipate energy in our model, which corresponds to wave breaking in the real world. The basic processes agree well with the experimental snapshots in Fig. 12 of Fritz et al. (2001).

4.5. Discussion

Tables 1–3 list predictions of wave crests, wave troughs, and runups by several numerical/experimental methods presented in the literature along with the results of the present study. The data extracted include arrival times, free surface elevation of crests/troughs, and runups at the gage position. To be consistent with the experimental results, the start times for all the numerical cases are switched to when the landslide just impacts the water surface. Relative errors are also given by comparison with experimental results.

From Tables 1 and 2, we find that only the present model and the VOF model (Basu et al., 2010) give all the free surface elevation for the six crests/troughs. The present model yields generally better predictions than the VOF method for the first three wave crests, and six troughs, however for the last three crests results from the VOF method seem a bit better than the present model's prediction. The level set method (Zhao et al., 2016) using a non-Newtonian landslide model only provides the free surface elevation for the first crest. The SPH method (Shi et al., 2016) provides free surface elevation for the first two crests and first trough that are better than those of the other methods. The better prediction of the first wave by the SPH model might be attributed to its consideration of the granular behavior of the landslide. Neither the level set nor SPH model even gave data for the other crests/troughs.

From Table 3, we also find that the present model gave better results than the VOF method for both arrival time and free surface elevation, but these were less accurate than the SPH predictions for the first runup. Since the layer-averaged model for water wave generation process has excluded some physical mechanisms such as impact and splash (Shi et al., 2016), which could also be found in Fig. 14(a-c), the runup of the LGIW obtained by the present model is lower than those models by three-dimensional Navier-Stokes models such as VOF and SPH.

We can summarize the abilities of these methods from the comparisons presented above. The three methods are all less satisfactory in describing topographic effects such as those of bed curvature and landslide dynamics because landslide physics is still poorly understood. However, the layer averaging in the two-layer method has been used in engineering, and SPH and PFEM could easily handle soil behavior because of their Lagrangian features. Thus, these methods have better ability than the VOF/LS method, which only considers a landslide as a multiphase flow or non-Newtonian fluid. The three methods can all handle the solid–fluid interaction in wave generation, but SPH/PFEM can model soil behavior a bit better than the other two methods. As for wave travel for a long time, the shallow-water or Boussinesq model combined with the two-layer method shows a better ability to model and control wave dissipation and dispersion than the other two methods, where the SPH/PFEM dissipation is even higher than that of the VOF/LS method. As for soil behavior, both the two-layer and VOF/LS models are weaker than the SPH/PFEM Lagrangian method. However, it should be noted that the layer averaging in the two-layer model has been used a lot in geological engineering algorithms for fast and even giant landslides. The two-layer method has lower numerical cost and can be better extended to 3D simulation than the other two methods. The ultimate aim of model development is application to the full process of a geological-scale LGIW in the real world. Therefore, currently only the two-layer method has turned out to be satisfactory for a geological-scale LGIW. Pudasaini (2012, 2014) and Gonzalez-Vida et al.(González-Vida et al., 2019) have developed two-layer models that can simulate the full process of a large-scale LGIW, but these are still weak in model-
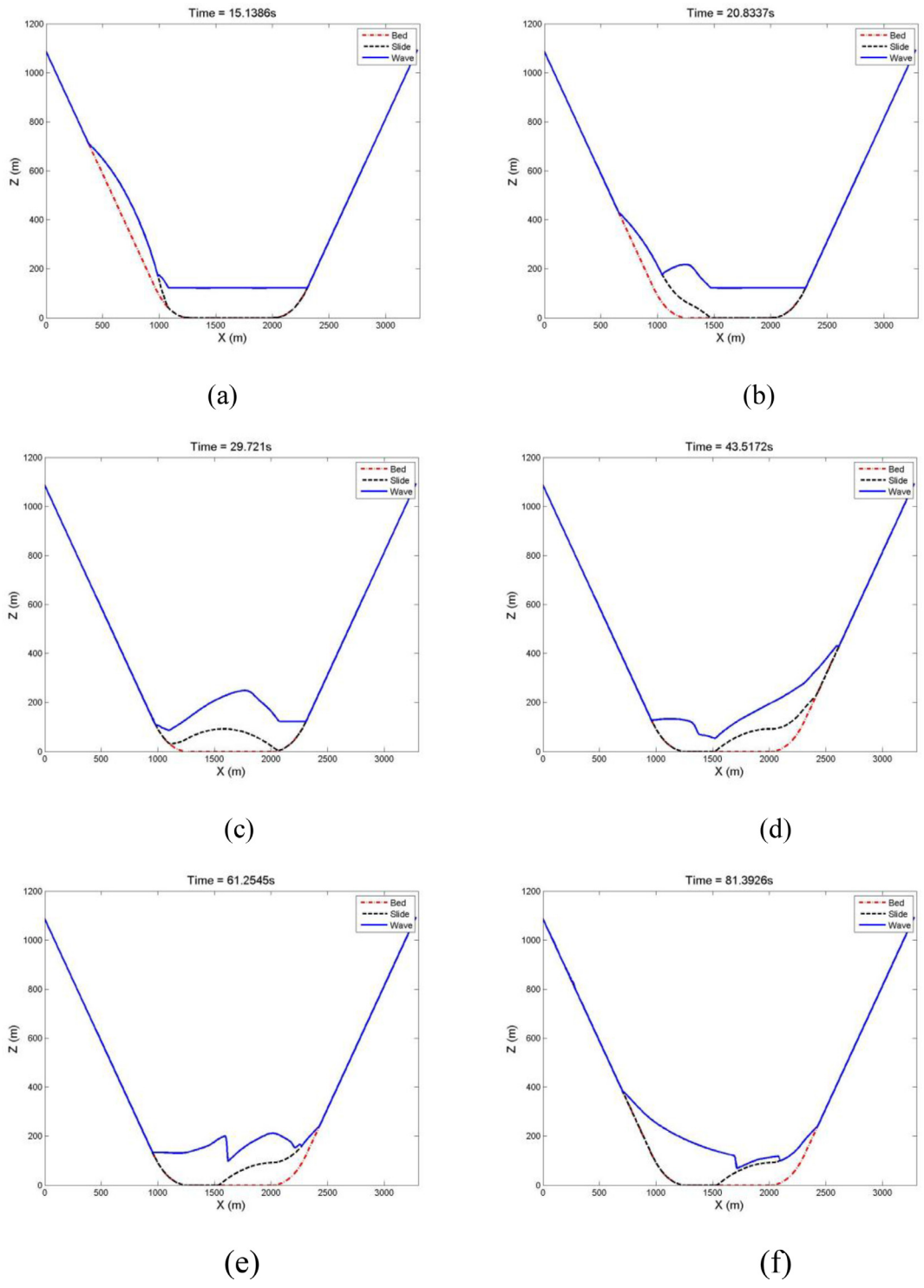
Fig. 14. Wave generation, runup, and back-flow processes in the Lituya LGIW.

Table 1
Free surface elevation data for the six crests of the Lituya LGIW from several methods. Experiment (Fritz et al., 2001), VOF (Basu et al., 2009), SPH (Shi et al., 2016), Level Set (Zhao et al., 2016)

	Cases	Wave Crests					
		1	2	3	4	5	6
Time Arrival(s)	Experiment 2001	16.00	47.55	92.25	127.86	178.91	213.37
(Relative Error%)	Present	16.00 (0.00)	47.78 (0.48)	87.50 (5.15)	115.43 (9.72)	162.30 (9.28)	190.67 (10.64)
	VOF 2009	16.00 (0.00)	42.56 (10.49)	90.32 (2.09)	114.44 (10.50)	155.38 (13.15)	186.57 (12.56)
	SPH 2016	15.57 (2.69)	46.73 (1.72)	—	—	—	—
	Level Set 2016	16.00 (0.00)	—	—	—	—	—
Elevation(m)	Experiment 2001	149.58	85.42	110.20	72.55	55.58	56.09
(Relative Error%)	Present	129.91 (13.15)	78.20 (8.45)	89.84 (18.48)	95.45 (31.56)	80.68 (45.16)	95.90 (70.98)
	VOF 2009	201.15 (34.48)	47.18 (44.77)	1.80 (98.37)	79.35 (9.37)	68.44 (23.14)	93.14 (66.05)
	SPH 2016	156.70 (4.76)	76.34 (10.63)	—	—	—	—
	Level Set 2016	235.16 (57.21)	—	—	—	—	—

Table 2
Free surface elevation data for the six troughs of the Lituya LGIW from several methods. Experiment (Fritz et al., 2001), VOF (Basu et al., 2009), SPH (Shi et al., 2016), Level Set (Zhao et al., 2016)

	Cases	Wave Troughs					
		1	2	3	4	5	6
Time Arrival(s)	Experiment 2001	29.15	73.47	106.71	145.95	192.90	230.27
(Relative Error%)	Present	36.48 (25.15)	81.01 (10.26)	110.17 (3.24)	149.83 (2.66)	182.97 (5.15)	225.67 (2.00)
	VOF 2009	25.75 (11.66)	66.56 (9.41)	104.94 (1.66)	147.82 (1.28)	173.29 (10.17)	210.20 (8.72)
	SPH 2016	34.41 (18.04)	—	—	—	—	—
	Level Set 2016	—	—	—	—	—	—
Elevation(m)	Experiment 2001	32.84	−22.32	12.54	−0.62	11.28	−0.47
(Relative Error%)	Present	24.55 (25.24)	−20.61 (7.66)	−2.55 (120)	9.98 (1709)	18.89 (67.46)	18.85 (4110)
	VOF 2009	−18.31 (155)	−112.53 (404)	−43.02 (443)	−44.74 (7116)	173.29 (73.94)	−20.60 (4285)
	SPH 2016	20.09 (38.82)	—	—	—	—	—
	Level Set 2016	—	—	—	—	—	—

Table 3
Runup of the Lituya LGIW from several methods. Experiment (Fritz et al., 2001), VOF (Basu et al., 2009), SPH (Shi et al., 2016)

	Cases	Runup		
		1	2	3
Time Arrival(s) (Relative Error%)	Experiment 2001	36.00	111.07	200.71
	Present	36.65 (1.81)	105.60 (4.92)	180.11 (10.26)
	VOF 2009	36.02 (0.06)	101.14 (8.94)	169.99 (15.31)
	SPH 2016	32.36 (10.11)	—	—
	Level Set 2016	—	—	—
Runup(m) (Relative Error%)	Experiment 2001	523.58	291.14	194.18
	Present	429.19 (18.03)	266.84 (8.35)	214.48 (10.45)
	VOF 2009	769.55 (46.98)	316.96 (8.87)	325.26 (67.50)
	SPH 2016	528.44 (0.93)	—	—
	Level Set 2016	—	—	—

ing the landslide dynamics of solid–fluid interaction. A cascade method linking SPH/PFEM and the two-layer method together might to some extent enhance modeling of the whole LGIW process.

5. Conclusion

(1) We proposed a new one-dimensional two-layer coupled model along with a computational algorithm to simulate the full process of a landslide-generated impulse wave. A reconstruction and interpolation scheme was developed to couple the shallow-water solver and landslide dynamics to realize the computation.

(2) The 1958 Lituya LGIW was reproduced by the proposed model for a whole duration of 250 s. The simulation captured six crests and troughs in the channel at a gage point, along with the runup on the right bank. These were comparable with experimental results. This seems to be the first reproduction of the 1958 Lituya LGIW for the whole physical process including wave generation, propagation, runup, and back flow by numerical simulation.

(3) We compared our model with three other models (another two-layer model, an interface-capture model, and a mesh-free/particle model) for an LGIW. The comparison included six important aspects including landslide modeling, wave generation, long-time wave transport, soil-behavior modeling, numerical cost, and geological-scale application. The proposed model exhibited a better ability than the other methods to simulate an LGIW from generation to long-duration travel in a unified framework.

Further work will include extending the current model to two dimensions and examining the effects of landslide deformation and dispersion of water waves. A cascade model linking SPH/PFEM for wave generation and depth averaging for wave transport is another important aim in this field.

Declaration of Competing Interest

The authors declare that they have no known competing financial interests or personal relationships that could have appeared to influence the work reported in this paper.

CRediT authorship contribution statement

Qingquan Liu: Investigation, Data curation, Writing – original draft. **Menghan Pan:** Software, Investigation, Visualization. **Xiaoliang Wang:** Supervision, Methodology, Conceptualization, Funding acquisition. **Yi An:** Data curation, Visualization.

Acknowledgements

References

Audusse, E., Bouchut, F., Bristeau, M.O., Klein, U., Perthame, B., 2004. A Fast and Stable Well-Balanced Scheme with Hydrostatic Reconstruction for Shallow Water Flows. SIAM J. Sci. Comput. 25 (6), 2050–2065. https://doi.org/10.1137/S1064827503431090, http://dx.doi.org/.

Basu, D., Green, S., Das, K., Janetzke, R., Stamatakos, J., 2009. Numerical Simulation of Surface Waves Generated by a Subaerial Landslide at Lituya Bay, Alaska. OMAE2009-79595, pp. 369–382. https://doi.org/10.1115/OMAE2009-79595

Billingham, J., King, A.C., 2000. Wave Motion. Cambridge University Press.

Blasio, F.V., 2011. Introduction to the Physics of landslides: Lecture Notes On the Dynamics of Mass Wasting. Springer Science & Business Media.

Bosa, S., Petti, M., 2011. Shallow water numerical model of the wave generated by the Vajont landslide. Environ. Modell. Softw. 26 (4), 406–418. https://doi.org/10.1016/j.envsoft.2010.10.001.

Castro-Orgaz, O., Hutter, K., Giraldez, J., Hager, W.H., 2015. Nonhydrostatic granular flow over 3-D terrain: new Boussinesq-type gravity waves? J. Geophys. Res. 120 (1), 1–28.

Fritz, H.M., Hager, W.H., Minor, H.E., 2001. Lituya Bay case: rockslide impact and wave runup. Sci. Tsunami Hazards 19 (1), 3–22.

Fritz, H.M., 2002. Initial Phase of Landslide Generated Impulse Waves. ETH.

González-Vida, J.M., Macías, J., Castro, M.J., Sánchez-Linares, C., Ortega, S., 2019. The Lituya Bay landslide-generated mega-tsunami – numerical simulation and sensitivity analysis. Nat. Hazards Earth Syst. Sci. 19, 369–388.

Heller, V., 2007. Landslide Generated Impulse Waves-Prediction of Near Field Characteristics. ETH.

Huang, C., Liu, Q.Q., Wang, X.L., 2020. Mechanism of peak discharge enhancement of cascade dam break floods. Chinese Journal of Theoretical and Applied Mechanics 52 (3), 645–655. https://doi.org/10.6052/0459-1879-20-044.

Iverson, R.M., Reid, M.E., LaHusen, R.G., 1997. Debris-flow mobilization from landslides. Annu. Rev. Earth Planet. Sci. 25 (1), 85–138. https://doi.org/10.1146/annurev.earth.25.1.85.

Kurganov, A., Petrova, G., 2007. A second-order well-balanced positivity preserving central-upwind scheme for the Saint-Venant system. Commu. Math Sci. 5 (1), 133–160. https://doi.org/10.4310/cms.2007.v5.n1.a6.

Kurganov, A., Miller, J., 2014. Central-Upwind Scheme for Savage–Hutter Type Model of Submarine Landslides and Generated Tsunami Waves. Comput. Meth. Appl. Mat. 14 (2), 177–201.

Lanne, D., 2013. The Water Waves Problem: Mathematical Analysis and Asymptotics. American Mathematical Society.

Li, J., Cao, Z.X., Liu, Q.Q., 2019. Waves and Sediment Transport Due to Granular Landslides Impacting Reservoirs. Water Resour. Res. 55 (1), 495–518.

Liang, Q.H., Marche, F., 2009. Numerical resolution of well-balanced shallow water equations with complex source terms. Adv. Water. Resour. 32 (6), 873–884. https://doi.org/10.1016/j.advwatres.2009.02.010.

Ma, G.F., Kirby, J.T., Hsu, T.J., Shi, F.Y., 2015. A two-layer granular landslide model for tsunami wave generation: theory and computation. Ocean. Model. 93, 40–55. https://doi.org/10.1016/j.ocemod.2015.07.012.

Mao, J., Zhao, L.H., Di, Y.T., Liu, X.N., Xu, W.Y., 2020. A resolved CFD-DEM approach for the simulation of landslides and impulse waves. Comput. Method. Appl. M. 359, 112750.

McFall, B.C., Fritz, H.M., 2016. Physical modelling of tsunamis generated by three-dimensional deformable granular landslides on planar and conical island slopes. P. Roy. Soc. A-Math Phys. 472, 20160052.

Mohammed, F., Fritz, H.M., 2012. Physical modeling of tsunamis generated by three-dimensional deformable granular landslides. J. Geophys. Res. 117, C11015.

Ni, Y.F., Cao, Z.X., Liu, Q.Q., 2019. Mathematical modeling of shallow water flows on steep slopes. J. Hydrol. Hydromech. 67 (3), 252–259.

Pudasaini, S.P., 2012. A general two-phase debris flow model. J. Geophys. Res. 117 (F3), 3010. https://doi.org/10.1029/2011jf002186, -.

Pudasaini, S.P., 2014. Dynamics of submarine debris flow and tsunami. Acta Mech. 225 (8), 2423–2434. https://doi.org/10.1007/s00707-014-1126-0.

Pudasaini, S.P., Hutter, K., 2007. Avalanche dynamics: Dynamics of Rapid Flows of Dense Granular Avalanches. Springer.

Quecedo, M., Pastor, M., Herreros, M.I., 2004. Numerical modelling of impulse wave generated by fast landslides. Int. J. Numer. Meth. Eng. 59 (12), 1633–1656. https://doi.org/10.1002/nme.934.

Salazar, F., Irazábal, J., Larese, A., Oñate, E., 2016. Numerical modelling of landslide-generated waves with the particle finite element method (PFEM) and a non-Newtonian flow model. Int. J. Numer. Anal. Met. 40 (6), 809–826.

Savage, S.B., Hutter, K., 1989. The motion of a finite mass of granular material down a rough incline. J. Fluid Mech. 199 (-1), 177–215. https://doi.org/10.1017/s0022112089000340.

Shi, C.Q., An, Y., Wu, Q., Liu, Q.Q., Cao, Z.X., 2016. Numerical simulation of landslide-generated waves using a soil–water coupling smoothed particle hydrodynamics model. Adv. Water. Resour. 92, 130–141 (jun.).

Tinti, S., Bortolucci, E., Chiavettieri, C., 2001. Tsunami excitation by submarine slides in shallow-water approximation. Pure Appl. Geophys. 158 (4), 759–797. https://doi.org/10.1007/pl00001203.

Wang, X.L., Li, J.C., 2017. A new solver for granular avalanche simulation: indoor experiment verification and field scale case study. Sci. China. Phys. Mech. (12), 124712.

Wang, X.L., Liu, Q.Q., 2021. Modeling shallow geological flows on steep terrains using a specific differential transformation. Acta Mech. 2021 232, 2379–2394. https://doi.org/10.1007/s00707-021-02944-3, https://doi.org/.

Wang, X.L., Shi, C.Q., Liu, Q.Q., An, Y., 2021. Numerical study on near-field characteristics of landslide-generated impulse waves in channel reservoirs. J. Hydrol. 2021 595, 126012.

Weiss, R., Fritz, H.M., Wünnemann, Kai., 2009. Hybrid modeling of the mega-tsunami runup in Lituya Bay after half a century. Geophys. Res. Lett. 36 (9), L09602. https://doi.org/10.1029/2009gl037814.

Yang, S., Wang, X.L., Liu, Q.Q., Pan, M.H., 2020. Numerical simulation of fast granular flow facing obstacles on steep terrains. J. Fluid. Struct. 99, 103162.

Zhao, L.H., Mao, J., Bai, X., Liu, X.Q., Li, T.C., Williams, J.J.R., 2016. Finite element simulation of impulse wave generated by landslides using a three-phase model and the conservative level set method. Landslides 13 (1), 85–96.